# Zirconium Bis(indenyl) Sandwich Complexes with an Unprecedented Indenyl Coordination Mode and Their Role in the Reactivity of the Parent Bent-Metallocenes: A Detailed DFT Mechanistic Study

**Luis F. Veiros*[a]**

**Abstract:** The mechanisms of three closely related reactions were studied in detail by means of DFT/B3LYP calculations with a VDZP basis set. Those reactions correspond to 1) the reductive elimination of methane from [Zr($\eta^5$-Ind)$_2$($CH_3$)(H)] (Ind = $C_9H_7^-$, indenyl), 2) the formation of the THF adduct, [Zr($\eta^5$-Ind)($\eta^6$-Ind)(thf)] and 3) the interconversion between the two indenyl ligands in the Zr sandwich complex, [Zr($\eta^5$-Ind)($\eta^9$-Ind)], which forms the link between the two former reactions. An analysis of the electronic structure of this species indicates a saturated 18-electron complex. A full understanding of the indenyl interchange process required the characterisation of several isomers of the Zr–bis(indenyl) species, corresponding to different spin states ($S=0$ and $S=1$), different coordination modes of the two indenyl ligands ($\eta^5/\eta^9$, $\eta^5/\eta^5$ and $\eta^6/\eta^9$), and three conformations for each isomer (*syn*, *anti*, and *gauche*). The fluxionality observed was found to occur in a mechanism involving bis($\eta^5$-Ind) intermediates, and the calculated activation energy (11–14 kcal mol$^{-1}$) compares very well with the experimental values. Two alternative mechanisms were explored for the reductive elimination of methane from the methyl/hydride complex. In the more favourable one, the initial complex, [Zr($\eta^5$-Ind)$_2$($CH_3$)(H)], yields [Zr($\eta^5$-Ind)$_2$] and methane in one crucial step, followed by a smooth transition of the Zr intermediate to the more stable $\eta^5/\eta^9$-species. The overall activation energy calculated ($E_a$ = 29 kcal mol$^{-1}$) compares well with experimental values for related species. The formation of the THF adduct follows a one step mechanism from the appropriate conformer of the [Zr($\eta^5$-Ind)($\eta^9$-Ind)] complex, producing easily ($E_a$ = 6.5 kcal mol$^{-1}$) the known product, [Zr($\eta^5$-Ind)($\eta^6$-Ind)(thf)], a species previously characterised by X-ray crystallography. This complex was found to be trapped in a potential well that prevents it from evolving to the 3.4 kcal mol$^{-1}$ more stable isomer, [Zr($\eta^5$-Ind)$_2$(thf)], with both indenyl ligands in a $\eta^5$-coordination mode and a spin-triplet state ($S=1$).

**Keywords:** density funtional calculations · indenyl ligands · reaction mechanisms · sandwich complexes · zirconium

## Introduction

Transition-metal sandwich complexes play a major role in modern organometallic chemistry, since its boom with the discovery of ferrocene.[1] A general interest in Group 4 metal sandwich compounds exists, given their participation in important reactions, such as catalytic processes,[2] small molecule activation[3] and organic coupling reactions.[2,4] However, few examples of fully characterised sandwich compounds of low-valent Group 4 metals are known, given their high reactivity that can activate cyclopentadienyl C–H bonds[5] or even inert molecules such as dinitrogen.[3a,6] In fact, the only examples published until the present are titanium compounds of cyclopentadienyl ligands with bulky substituents ($C_5Me_4R^-$).[7–9] Analogous species with zirconium and hafnium have been more elusive and their attempted synthesis unsuccessful, probably due to the known tendency of those metals to attain their highest oxidation states and, thus, the relative instability of the corresponding low-valent complexes. Nevertheless, the presence of zirconocene intermediates, [ZrCp′$_2$] (Cp′ = substituted cyclopentadienyl), has been hinted by a number of studies, including its role in catalytic processes[2] and trapping with donor ligands or even dinitrogen.[10–12]

[a] Prof. L. F. Veiros
Centro de Química Estrutural
Instituto Superior Técnico
1049-001 Lisboa (Portugal)
Fax: (+351) 21-846-4455
E-mail: veiros@ist.utl.pt

Supporting information for this article is available on the WWW under http://www.chemeurj.org/ or from the author. 1) Complementary data on the mechanism (Figures S1 to S4), and 2) atomic coordinates for all the optimised species.

 **DOI: 10.1002/chem.200401235**  

Indenyl ($Ind = C_9H_7^-$) is a versatile ligand that can coordinate a metal centre in diverse modes,[13] corresponding to the formation of a different number of M–C bonds. This is named the *hapticity* and is usually denoted by the symbol η. The most common coordination mode of that ligand is $\eta^5$-Ind, corresponding to the presence of five bonds between the metal and the carbon atoms of the $C_5$ ring, similar to what happens in a $\eta^5$-cyclopentadienyl ($Cp = C_5H_5^-$) complex. Indenyl has been widely used in the place of cyclopentadienyl, opening many new and, in some cases, surprising routes in metallocene chemistry. The ability of indenyl to change its coordination mode, adjusting to the metal electronic needs, confers the corresponding complexes an enhanced reactivity towards ligand substitution reactions giving rise to the expression "indenyl effect".[14]

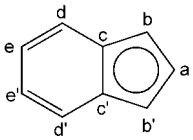

Indenyl

In a very recent work, Chirik et al. identified and characterised in solution a $[Zr(Ind')_2]$ sandwich complex,[15] corresponding to the intermediate in the sequence of reactions represented in Scheme 1. In the first reaction there is a reductive elimination of an alkane from an alkyl/hydride complex, and, in the second, the formation of a THF adduct. Solution molecular-weight determination and NMR data allowed the identification of the intermediate as the species represented in Scheme 1. This species, with two nonequivalent indenyl ligands, was formulated as $[Zr(\eta^5\text{-Ind}')(\eta^6\text{-Ind}')]$ given the shift on the coordination mode of one of the indenyl ligands from the $\eta^5$-mode, existing in the parent alkyl/hydride complex, to $\eta^6$-Ind coordinated by the benzene ring in the final THF adduct. The bonding geometry of the Ind ligands in the THF adduct was clearly established by the determination of the corresponding X-ray structure. This extraordinary result prompted the work described here.

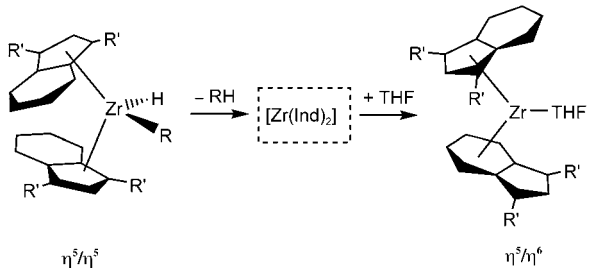

Scheme 1.

In this work, DFT calculations[16] are used to perform a twofold goal. On the one hand, the thorough investigation of the nature of the $[Zr(Ind)_2]$ species, and the mechanism for the interconversion between the two differently coordinated ligands in this species and on the other, the elucidation of the mechanisms of the two reactions represented in Scheme 1.

## Results and Discussion

**The zirconium sandwich complex, $[Zr(Ind)_2]$**: The optimisation of the geometry of a $[Zr(Ind)_2]$ complex was accomplished by means of B3LYP calculations[17–19] with a VDZP basis set (see Computational Methods). In the obtained molecule (Figure 1) one of the indenyl ligands is coordinated in the usual $\eta^5$-mode, while the second ligand is severely bent over the central $C_c$–$C_{c'}$ bond so that all its nine carbon atoms approach the metal in an unprecedented $\eta^9$-coordination mode (see above for the labelling of the indenyl carbon atoms).

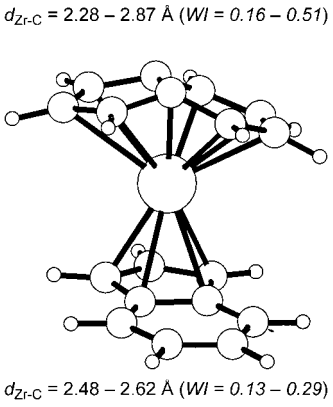

Figure 1. Optimised geometry (B3LYP/VDZP) of a $[Zr(\eta^5\text{-Ind})(\eta^9\text{-Ind})]$ complex. The range of Zr–C bond lengths (Å) and the corresponding Wiberg indices (WI, italics) are indicated.

It should be noted that during the course of the work here described, structures of $[Zr(\eta^5\text{-Ind}')(\eta^9\text{-Ind}')]$ complexes with indenyl ligands substituted in the $C_b$ and $C_{b'}$ positions have been experimentally determined by X-ray crystallography in an independent work developed in Paul Chirik's group.[20] Besides the structural data, the results reported include a kinetic study of the fluxional process corresponding to the interconversion between the two Ind ligands with determination of the activation parameters, its dependence on the Ind substituents and the reactivity of the $[Zr(Ind)_2]$ complexes with unsaturated organic molecules.

The geometry calculated for $[Zr(\eta^5\text{-Ind})(\eta^9\text{-Ind})]$, and represented in Figure 1, compares well with the experimental structure, especially considering that in the latter the two indenyl ligands have isopropyl groups attached to $C_b$ and $C_{b'}$[20] (see Table 1). The experimental $d_{Zr-C}$ distances range from 2.48 to 2.54 Å for the five-coordinate atoms in $\eta^5$-Ind, and from 2.27 to 2.78 Å for the $\eta^9$-coordinate ligand. The corresponding optimised range of values are represented in Figure 1. The calculated angles are also in good agreement with the experimental values. For example, the practically linear arrangement, ct($\eta^5$)-Zr-ct($\eta^9$), experimentally verified (174°) is well reproduced by the calculations (175°). The parameters ct($\eta^x$) will be used throughout the text to denote the "coordination midpoint" of the Ind ligand in the different modes, corresponding to the centroid of the $C_5$ ring for

Table 1. Experimental[a] (in parenthesis) and calculated Zr–C coordination distances [Å] for the [Zr($\eta^5$-Ind)($\eta^9$-Ind)] complex.

| Zr–C | $\eta^5$-Ind | $\eta^9$-Ind |
|---|---|---|
| $C_a$ | 2.501 (2.517) | 2.869 (2.784) |
| $C_b$ | 2.516 (2.536) | 2.666 (2.574) |
| $C_{b'}$ | 2.481 (2.485) | 2.637 (2.626) |
| $C_c$ | 2.624 (2.539) | 2.293 (2.255) |
| $C_{c'}$ | 2.606 (2.528) | 2.280 (2.267) |
| $C_d$ | – | 2.412 (2.334) |
| $C_{d'}$ | – | 2.391 (2.386) |
| $C_e$ | – | 2.552 (2.487) |
| $C_{e'}$ | – | 2.543 (2.501) |

[a] In the experimental structure the two indenyl ligands have isopropyl groups attached to $C_b$ and $C_{b'}$.

a $\eta^5$-Ind ligand, the centroid of the benzene ring for a $\eta^6$-coordination, and the midpoint of the $C_c$–$C_{c'}$ bond for a $\eta^9$-geometry. The rotational angle between two indenyl ligands in a bis(indenyl) species, with one $\eta^x$-Ind and one $\eta^y$-Ind, may be defined as the torsional angle $\langle C_e–C_{e'}\rangle$-ct($\eta^x$)-ct($\eta^y$)-$\langle C_e–C_{e'}\rangle$, in which $\langle C_e–C_{e'}\rangle$ is the midpoint of the $C_e$–$C_{e'}$ bond in each ligand. In the [Zr($\eta^5$-Ind)($\eta^9$-Ind)] molecule this angle ($\beta$, see Scheme 2) reflects a *gauche*-conformation of the molecule; its calculated value (89°) compares well with the experimental value (85°). The most striking geometrical feature of the Ind coordinated in a $\eta^9$-mode is, perhaps, the fold angle ($\alpha$) observed between the plane of the $C_5$ ring and the plane of the benzene ring. This can be define as the angle $C_a$-ct($\eta^9$)-$\langle C_e–C_{e'}\rangle$, and the agreement between the optimised value (146°) and the experimental one (142°) is also good.

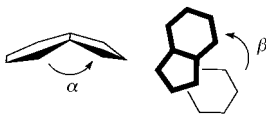


Scheme 2.

If the Ind coordinated in a $\eta^9$-fashion is fully engaged in the bonding to the metal, then the species [Zr($\eta^5$-Ind)($\eta^9$-Ind)] corresponds to a saturated 18-electron complex. This somehow surprising result, taking into account that it is a complex with a Group 4 metal and only two indenyl ligands, is confirmed by a deeper analysis of the electronic structure of the molecule. The $d_{Zr–C}$ distances obtained for the $\eta^9$-Ind ligand are within the bonding range, although some are on the long side, and are comparable to the ones optimised for the "normal" $\eta^5$-ligand (see Figure 1). The longer Zr–C distances correspond to $C_b$ and $C_{b'}$, 2.64 and 2.67 Å, and $C_a$, 2.87 Å; all the bond lengths to the benzene ring are within 2.55 Å (Zr–$C_{e/e'}$). The values of the previous distances could suggest the absence of significant bonds between the metal and the three allylic carbons of the $C_5$ ring, but some caution should be taken on a geometrical analysis based only in distances. In fact, the use of an electronic parameter such as the Wiberg index (WI),[21] a well-known bond-strength indicator, changes the previous picture in a substantial manner. Although Zr–$C_a$ corresponds to the longest bond length in the molecule, its Wiberg index (0.16) indicates the existence of a bond and is, in fact, higher than those found for the two bridgehead carbons ($C_c$ and $C_{c'}$) in the indenyl group coordinated in the usual $\eta^5$-mode ($WI_{Zr–C_{c/c'}}=0.13$), despite the shorter Zr–$C_{c/c'}$ bond lengths (2.61, 2.62 Å).

The coordination geometry of the $\eta^9$-Ind in the complex of Figure 1 is reminiscent of Group 4 pentalene compounds.[22] Pentalene ($C_8H_6^{2-}$) is formed by two $C_5$ rings fused by one C–C bond. However, the differences in symmetry between pentalene and indenyl and, consequently, the corresponding differences on the orbital characteristics of the two ligands,[23] make them different ligands. For example, pentalene was found to be only a 9-electron donor in [Ti($\eta^8$-$C_8H_6$)$_2$],[24] since the highest occupied molecular orbital (HOMO) of the ligands finds no symmetry match among the metal orbitals. Should the complex in Figure 1 be an 18-electron species, then the $\eta^9$-Ind must be a 10-electron donor. More interesting is the comparison between [Zr($\eta^5$-Ind)($\eta^9$-Ind)] and the bent zirconocene butadiene complex, [$ZrCp_2$(2,3-dimethylbutadiene)],[25] or its *ansa* analogues.[26] The bond lengths and Wiberg indices (italics) relevant for the comparison are present in Scheme 3a, for the bis(indenyl) complex.

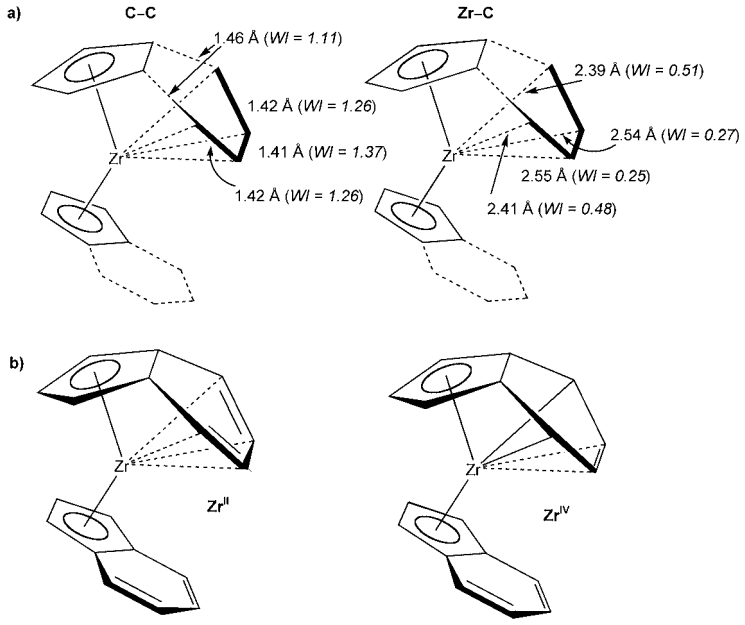


Scheme 3.

  

The overall coordination geometry of the benzo portion of the $\eta^9$-Ind ($C_{d/d'}$ and $C_{e/e'}$) in [Zr($\eta^5$-Ind)($\eta^9$-Ind)] is similar to what is found in the butadiene complexes. Nevertheless, a few subtle differences exist. In the butadiene species the coordination of this ligand approaches a metallocyclopentene,[25,26] with the establishment of two Zr–C σ bonds to the outer butadiene atoms and some C=C double-bond character between two inner ones. This tendency is attenuated in the bis(indenyl) complex, in which the coordination of the benzo portion the $\eta^9$-ligand is close to what would be a $\eta^4$-butadiene. This is better analysed by looking at the C–C bond lengths, since the Zr–C distances are affected by steric constraints absent in an "independent" butadiene, but present in the indenyl ligand, in which the benzo portion is attached to the $C_5$ ring. A clear tendency towards a bond alternation exists in [Zr{$Me_2C(C_5H_4)_2$}(butadiene)] with the butadiene C–C inner distance 0.07 Å shorter than the outer ones, while in [Zr($\eta^5$-Ind)($\eta^9$-Ind)] the corresponding difference is only 0.01 Å. In addition, the establishment of four Zr–C bonds between the metal and the benzo carbons of $\eta^9$-Ind is confirmed by values of the corresponding Wiberg indices, indicative of strong interactions (WI $\geq$ 0.25). In conclusion, the [Zr($\eta^5$-Ind)($\eta^9$-Ind)] complex can be described as intermediate between a $Zr^{II}$ $d^2$ species and a $Zr^{IV}$ $d^0$ molecule (Scheme 3b). In the former case, the benzo part of the $\eta^9$-Ind is equivalent to a neutral $\eta^4$-butadiene, while in the latter it corresponds to a dialkyl, a formally dianionic ligand.

The analogy with the butadiene complexes may be used to understand the saturated character of [Zr($\eta^5$-Ind)($\eta^9$-Ind)] by an analysis of the occupied frontier orbitals of this molecule. In fact, the orbitals represented in Figure 2 can be viewed as resulting from the combination of the well-known frontier orbitals of a bent metallocene fragment,[27] with the first three π orbitals of butadiene, similar to what has been found for Zr–butadiene complexes.[26] Thus, the HOMO of the bis(indenyl) complex results from the combination of metallocene $3a_1$ and butadiene $\pi_3$ orbitals, the HOMO−2 represents the mixture of metallocene $2b_1$ and butadiene $\pi_2$ orbitals and HOMO−4 derives from the combination of metallocene $4a_1$ orbital with the first butadiene π orbital, $\pi_1$. The three frontier orbitals of each fragment are involved in occupied molecular orbitals that accommodate the corresponding six electrons. The result is, formally, a pair of 2-electron donations from the benzo ring of Ind to Zr and a 2-electron backdonation from the metal to the ligand. This electronic structure confirms the saturated character of the molecule and, consequently, its description as an 18-electron complex. Moreover, the participation of $C_e$ and $C_{e'}$, and thus the $\eta^4$-character of the coordination of the benzo part in $\eta^9$-Ind, is verified in all orbitals of Figure 2, especially in HOMO−4. It should be noted that given the absence of symmetry in the molecule, the interactions represented in Figure 2 are, in fact, mixed with other interactions and participate in other molecular orbitals. The occupied molecular orbitals HOMO−1 and HOMO−3 also have bonding character between Zr and Ind, involving d orbitals of the metal and the π system of the ligands. Being not relevant to the discussion above they are not represented in Figure 2 for the sake of clarity.

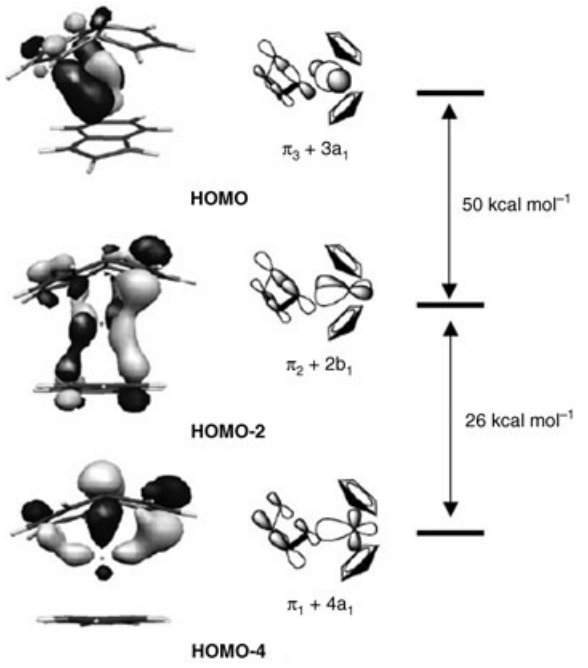


Figure 2. Occupied molecular orbitals of Zr($\eta^5$-Ind)($\eta^9$-Ind)] that can be viewed as formally resulting from the mixing of the frontier orbitals of a bent metallocene fragment and a butadiene. The relative energy of the orbitals (kcal mol$^{-1}$) is indicated.

The possible mechanisms for the Ind interconversion in [Zr($\eta^5$-Ind)($\eta^9$-Ind)], a process known to occur in solution,[20] are depicted in Scheme 4. The basic motions on the original $\eta^5/\eta^9$-complex (centre of Scheme 4) correspond the dissociation of the benzo part of $\eta^9$-Ind (1), the dissociation the allylic part of the $C_5$ ring of the same ligand (2) and the coordination of the benzo portion of the $\eta^5$-Ind (3). The simplest mechanism would be a concerted one with the simultaneous dissociation of the benzo part of $\eta^9$-Ind and coordination of the equivalent atoms in the $\eta^5$-ligand (1+3). This is mechanism **I** in Scheme 4. All the other possibilities involve a

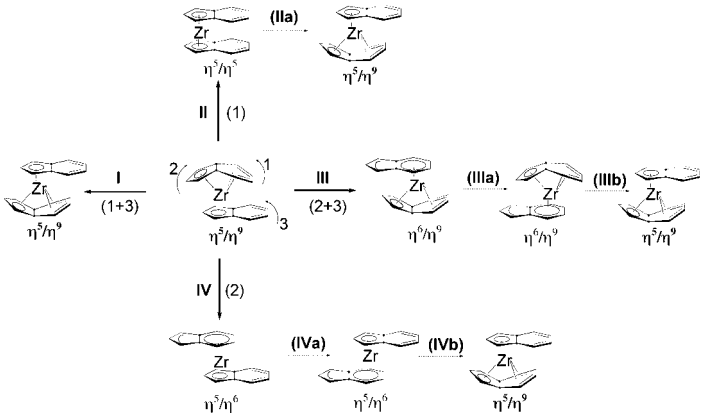


Scheme 4.

mechanism that follows two or more steps. Mechanism **II** corresponds to the dissociation of the benzo part of $\eta^9$-Ind leading to a bis($\eta^5$) species. This a symmetrical molecule, as far as the Ind coordination mode is concerned, and by following the same mechanism on the other Ind ligand will produce the $\eta^5/\eta^9$-species with exchanged ligands. Mechanisms **III** and **IV** involve the dissociation of $C_a$ and $C_{b/b'}$ on the five-membered ring of the $\eta^9$-Ind. In **III** this is compensated by the coordination of the benzene ring of the $\eta^5$-ligand, yielding an $\eta^6/\eta^9$-species, while in **IV** this does not happen and an $\eta^5/\eta^6$-complex is produced. These intermediates ($\eta^6/\eta^9$ or $\eta^5/\eta^6$) would, then, suffer the interconversion process in a second step and, finally, a third step, similar to the first one but involving the other ligand, produces the $\eta^5/\eta^9$-species with interchanged ligands.

Numerous attempts were made to obtain a transition state corresponding to a concerted mechanism (**I**) without success, suggesting that this is not the mechanism for the fluxional process observed. As previously noted,[20] this would correspond to an associative mechanism in an electronically saturated 18-electron complex, and, thus, an unlikely one. In fact, such a mechanism had to include a transition state with two symmetrically coordinated Ind, with a coordination geometry intermediate between $\eta^5$ and $\eta^9$. The HOMO of a model with those characteristics is depicted in Figure 3, showing the existence of antibonding interactions between the metal and the $C_{e/e'}$ atoms in the two ligands, and justifying why a concerted mechanism is unfavourable.

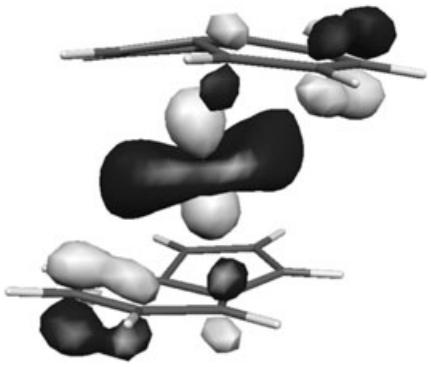

Figure 3. HOMO of a model with two symmetrically coordinated Ind with a coordination geometry intermediate between $\eta^5$ and $\eta^9$.

The investigation of a mechanism occurring in two or more steps must start by the identification of the intermediates involved. This was accomplished by a thorough search of the appropriate potential-energy surfaces (PES) allowing the optimisation of all the isomers in Scheme 4, with different indenyl coordination modes, namely, $\eta^5/\eta^9$-, $\eta^5/\eta^5$-, $\eta^6/\eta^9$- and $\eta^5/\eta^6$-[Zr(Ind)$_2$] complexes. It should be noted that two isomers with $\eta^5/\eta^5$-geometry were found; one with singlet spin state ($S=0$) and one with a more stable spin triplet ($S=1$). This and the relative stability of the different isomers will be addressed below, when discussing the mechanisms for the Ind interconversion. Three conformations were considered for each one of those isomers: *syn*, *gauche* and *anti* (see Scheme 5).

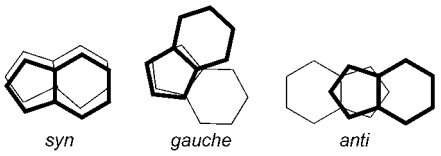


Scheme 5.

Given the number of isomers and conformers involved, an intuitive notation is used in which the first character denotes the conformation (**S** for *syn*, **G** for *gauche* and **A** for *anti*), and the two following numbers represent the hapticity of the two indenyl ligands. Thus, the $\eta^5/\eta^9$-complex in the *gauche*-conformation, represented in Figure 1 and discussed above, is **G59**. The three conformers for the $\eta^5/\eta^9$-species, as well as the energy profile for the indenyl rotation, are represented in Figure 4.

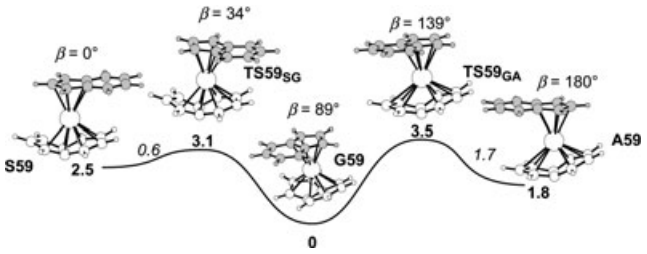


Figure 4. Energy profile for the rotation of indenyl in the $\eta^5/\eta^9$-[Zr(Ind)$_2$] complexes. The minima and the transition states were optimised (B3LYP/VDZP) and the obtained structures are presented. The energies (kcal mol$^{-1}$) are referred to the more stable conformer (*gauche*), and the values in italics represent energy barriers. The rotating indenyl is shaded and the rotation angle ($\beta$) is indicated for all the species.

The profile in Figure 4 indicates that the stability difference between the three conformers is minimal, within 2.5 kcal mol$^{-1}$. All the $\eta^5/\eta^9$-species are readily accessible, since rotation occurs smoothly with a maximum activation energy of 3.5 kcal mol$^{-1}$. This corroborates the experimental finding that the rotation does not stop, even after freezing the interconversion process.[20] The rotation occurs minimizing the energy costs as the coordination geometry of each ligand is maintained, and the transition states present rotation angles intermediate between the values obtained for the two corresponding minima. Interestingly, an X-ray structure has been determined for an *anti*-conformer of [Zr($\eta^5$-Ind′)($\eta^9$-Ind′)] with indenyl ligands substituted at the $C_{b/b'}$ atoms with $SiMe_2tBu$. This shows that the small energy differences between the conformers can easily be overtaken by the stereochemical influence of indenyl substituents or by crystal-packing effects. The calculated geometry for **A59** matches the experimental structure well, taking into consideration the differences between the ligands, with mean and maximum absolute deviations of 0.03 and 0.13 Å, respective-

  

ly, for the Zr–C bonds, and 2–3° differences for the relevant angles: α, β and ct($\eta^5$)-Zr-ct($\eta^9$). The energy profiles for the indenyl rotation in the other isomers, $\eta^5/\eta^5$ ($S=0$ and $S=1$), and $\eta^6/\eta^9$ are presented in Figure S1 in the Supporting Information. The energy barriers for the rotation increase as the isomer becomes less stable, the highest calculated value being 6.8 kcal mol$^{-1}$ for the $\eta^6/\eta^9$-species. The species with $\eta^5/\eta^6$-coordination, a spin triplet ($S=1$), was not considered, since it corresponds to the less stable isomer that is too destabilised with respect to **G59** to participate in the interconversion mechanism. The energy difference between the $\eta^5/\eta^6$-species and **G59** is 13.7–14.4 kcal mol$^{-1}$, for the three conformers, **S56**, **G56** and **A56**.

The stability differences of the isomers, with differing coordination of the two indenyl ligands, is better addressed in the context of the mechanisms obtained for the interconversion process, in which the isomers appear naturally as intermediates. The less stable isomer of [Zr(Ind)$_2$] present in the calculated mechanisms is the $\eta^6/\eta^9$-species (**G69**), the intermediate of mechanism **III** in Scheme 4. The calculated energy for **G69** is 13.4 kcal mol$^{-1}$ above **G59**. The difference between the two complexes is the presence of an indenyl coordinated in a $\eta^5$-mode in one molecule, and a $\eta^6$-Ind in the other; the second ligand is in both cases $\eta^9$-Ind. The reason for the stability difference may be found by an analysis the Zr–Ind bonds in both complexes (see Scheme 6). An $\eta^6$-coordinate Ind ligand establishes weaker bonds with the metal than $\eta^5$-Ind ligands, as suggested by the Zr–C Wiberg indices (WI = 0.14–0.25 for **G69**, and 0.13–0.29 for **G59**), and by the charges of the two ligands, obtained by means of a natural population analysis (NPA).[28] The $\eta^6$-Ind ligand in **G69** is more negative (−0.60) than the $\eta^5$-Ind ligand in **G59** (−0.49), showing that the ligand acts as a better donor in the latter case, and justifying a stronger bond to the metal. A synergetic effect occurs and the Zr–($\eta^9$-Ind) bond is also stronger in the $\eta^5/\eta^9$-species (**G59**), since the $\eta^5$-Ind pushes more electronic density to the metal and, thus, reinforces the backdonation from Zr to $\eta^9$-Ind moitey, as shown by the charges and WI in Scheme 6. The result is an overall gain in stability for the [Zr($\eta^5$-Ind)($\eta^9$-Ind)] isomer. The $\eta^5/\eta^5$-species have intermediate stability between the more stable [Zr($\eta^5$-Ind)($\eta^9$-Ind)] complexes and the $\eta^6/\eta^9$-isomers.

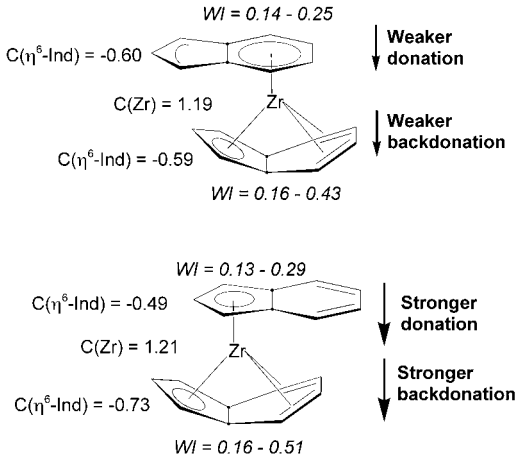


Scheme 6.

The indenyl interconversion mechanisms obtained for the *gauche*-conformers are represented in Figure 5. The corresponding energy profiles for the *syn*- and *anti*-conformers are presented in Figures S2 and S3 in the Supporting Information.

The energy profile for mechanism **III** (top of Figure 5) shows a mechanism in three steps. In the first, there is a simultaneous slippage of one ligand from $\eta^9$ to $\eta^6$ and of the other indenyl from $\eta^5$ to $\eta^9$, going from **G59** to the corresponding $\eta^6/\eta^9$-isomer, **G69**. In the second step the coordination mode of the two indenyl ligands in exchanged in **G69**, and in a final step, equivalent to first, the more stable form (**G59**) with interconverted coordination modes of the two indenyl ligands is produced. In the first transition state, **TS$_{G56–G69}$**, the dissociation of the allylic part of the $\eta^9$-Ind in the reactant **G59** is complete, as shown by a practically planar ligand with a long Zr–C$_a$ distance (4.02 Å). However, the second motion is far from finished, that is, the coordination of the benzo part of the originally $\eta^5$-coordinated Ind in **G59** (shaded in Figure 5) is only incipient, with long Zr–C$_{e/e'}$ distances (3.15, 3.19 Å) and corresponding weak interactions (WI = 0.08, 0.10). This indicates a dissociative nature for the mechanism, as expected for an 18-electron complex (see above). The second step, the interchange between the two ligands in **G69**, occurs through a transition state, **TS$_{G69}$**, with two indenyl ligands symmetrically coordinated in $\eta^6$-mode. Again, both ligands are essentially planar in **TS$_{G69}$** showing the dissociative nature of this step, as the bonds between the metal and the allylic part of the $\eta^9$-Ind in **G69** are broken prior to the formation of the equivalent bonds in the ligand changing from $\eta^6$ to $\eta^9$. The [Zr($\eta^5$-Ind)($\eta^9$-Ind)] with exchanged ligands is formed in a final step, equivalent to the first one. The overall activation energy for the mechanism is 20.8 kcal mol$^{-1}$. Interestingly, the dissociative nature of the mechanism allows the maintenance of the bonding character of the HOMO of the involved species, in contrast to what would happen in a concerted mechanism (see Figure 3 and its discussion above). The corresponding orbitals are presented in Figure S4 in the Supporting Information.

The mechanism corresponding to the profile in the bottom of Figure 5 involves $\eta^5/\eta^5$-intermediates, being mechanism **II** in Scheme 4. Two such intermediates were found, **$^3$G55** and **$^1$G55**, were the superscript denotes the spin multiplicity, given by 2S + 1, S being the total spin of the molecule. Although the two $\eta^5/\eta^5$-species are geometrically equivalent, with Zr-C distances within 0.02 Å and a difference of 1° between the ct($\eta^5$)-Zr-ct($\eta^5$) angles, the spin-triplet isomer, **$^3$G55**, is more stable than its singlet analogue by 2.7 kcal mol$^{-1}$, as expected for a d$^2$ metallocene.[27] A reaction path from **G59** to the more stable of the $\eta^5/\eta^5$-intermediates, **$^3$G55**, is in fact a "spin forbidden" one and has to go through a minimum-energy crossing point (MECP) of

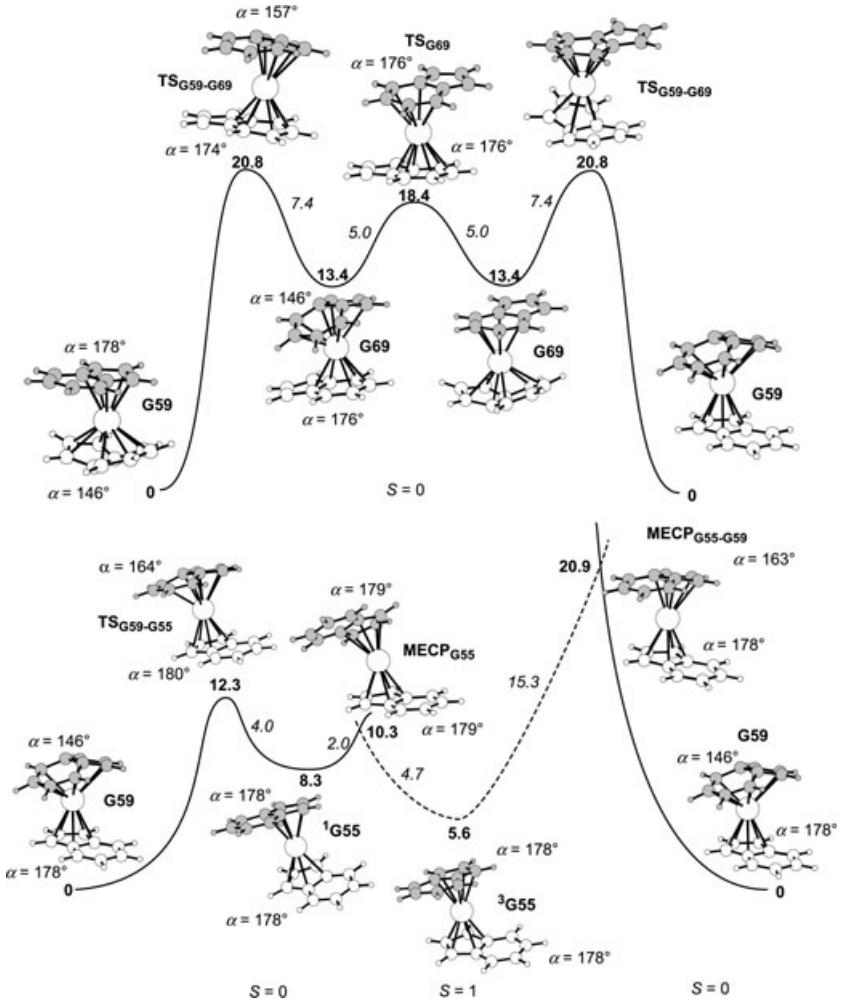


Figure 5. Energy profiles for the interconversion mechanisms of the two indenyl ligands in [Zr($\eta^5$-Ind)($\eta^9$-Ind)] in the *gauche*-conformation. Mechanism **II** (bottom) involves $\eta^5/\eta^5$-intermediates, and mechanism **III** (top) goes through the $\eta^6/\eta^9$-isomer. The relevant points were optimised (B3LYP/VDZP) and the obtained structures are presented. The energies (kcal mol$^{-1}$) are referred to the more stable conformer (**G59**), and the values in italics represent energy barriers. One indenyl is shaded and the fold angle ($\alpha$) is indicated for all the species. The plain curves correspond to the spin-singlet ($S=0$) PES and the dashed curve to the spin-triplet ($S=1$) PES.

the two potential-energy surfaces (PES), that is, the spin singlet and the triplet surfaces. This corresponds to the lowest energy point at which the geometry and the energy of the molecule in the two surfaces are the same. Once that point is reached, the system has a given probability of changing its spin state and hops from one surface to the other, giving rise to the corresponding "non-adiabatic" or "spin-forbidden" reaction.[29] This is illustrated on the right part of the bottom profile in Figure 5 for the reaction that converts directly **G59** in $^3$**G55**. In the corresponding MECP, **MECP$_{G55-G59}$**, the slipping indenyl has a fold angle (163°) intermediate between the one found in the $\eta^9$-Ind existing in **G59** and the flat $\eta^5$-ligand of $^3$**G55**. Another possibility is the participation of the singlet $\eta^5/\eta^5$-species $^1$**G55** in the mechanism. This process corresponds a slippage of one ligand in the reactant (**G59**) from $\eta^9$- to $\eta^5$-coordination, with the reaction occurring in the spin-singlet PES. The $^1$**G55** intermediate is reached through a transition state **TS$_{G59-G55}$**, in which the unfolding ligand has a coordination mode in between $\eta^9$ and $\eta^5$ ($\alpha=164°$), and an activation energy of 12.3 kcal mol$^{-1}$, being significantly smaller than the one involved in a direct transformation from **G59** in $^3$**G55** (20.9 kcal mol$^{-1}$). Thus, the most favourable process to reach a bis($\eta^5$) complex from the $\eta^5/\eta^9$-molecule involves the singlet intermediate $^1$**G55**. This is also the first step of the mechanism for the Ind interconversion in [Zr($\eta^5$-Ind)($\eta^9$-Ind)] with lower activation energy. In fact, an interconversion mechanism for the two ligands in [Zr($\eta^5$-Ind)($\eta^9$-Ind)] involving the $\eta^5/\eta^5$-intermediates ($^1$**G55** and $^3$**G55**) is conceptually simple. Once these intermediates are reached, the coordination mode of the two ligands is equivalent and the interchange may occur by following the same process with the second ligand (**IIa** in Scheme 4). From the singlet $\eta^5/\eta^5$-species ($^1$**G55**) the system only has to overcome a 2.0 kcal mol$^{-1}$ barrier to yield the corresponding triplet analogue $^3$**G55**. The geometrical similarity between the two molecules makes the corresponding MECP (**MECP$_{G55}$**) easy to reach and, in fact, easier than **TS$_{G59-G55}$**. However, even if $^1$**G55** yields $^3$**G55** more easily than **G59**, at least in activation energy terms, the mechanism for the interconversion has to follow the same route back, going through **MECP$_{G55}$**, given the high energy of **MECP$_{G55-G59}$**. In the case of Figure 5 this corresponds to the following sequence: **G59**→**TS$_{G59-G55}$**→$^1$**G55**→**MECP$_{G55}$**→$^3$**G55**→**MECP$_{G55}$**→$^1$**G55**→**TS$_{G59-G55}$**→**G59**. Interestingly, this is also a dissociative mechanism, since the $\eta^9$-Ind ligand dissociates its benzo portion from the metal, while the second ligand remains $\eta^5$-coordinate. In this process the HOMO of **G59** changes from a bonding orbital (Figure 2) to a metal-centred nonbonding one, the known $3a_1$ of a metallocene,[27] avoiding the antibonding interaction that would occur in a concerted mechanism (see Figure 3). The HOMO of the more relevant species **G59**, **TS$_{G59-G55}$** and $^1$**G55**, are represented in Figure S4 in the Supporting Information.

  

Similar conclusions may be drawn from the energy profiles involving the two other conformations of the complex, *syn* and *anti* (see Figures S2 and S3 in the Supporting Information). In all cases the most favourable path for the Ind interconversion in [Zr($\eta^5$-Ind)($\eta^9$-Ind)] is a mechanism with the $\eta^5/\eta^5$-complexes as intermediates. The calculated activation parameters for the process, all conformations considered ($\Delta H^{\neq} = 11.3$–$13.4$ kcal mol$^{-1}$ and $\Delta G^{\neq}_{298} = 10.5$–$12.4$ kcal mol$^{-1}$), compare very well with the experimental values determined for [Zr($\eta^5$-Ind′)($\eta^9$-Ind′)] with indenyl substituted in the $C_{b/b'}$ positions: $\Delta H^{\neq} = 14.5$–$20.4$ kcal mol$^{-1}$ and $\Delta G^{\neq}_{296} = 13.8$–$16.9$ kcal mol$^{-1}$.[20]

**Methane reductive elimination from [Zr(Ind)$_2$(Me)(H)]**: A [Zr(Ind′)$_2$] species such as the one discussed above was first identified following the alkane reductive elimination of a alkyl hydride complex, [Zr(Ind′)$_2$(X)(H)].[15] In this work, a model with nonsubstituted indenyl ligands and methyl as the alkyl ligand, X, is used in order to study the mechanism of this reaction. The optimised structure obtained for [Zr(Ind)$_2$(Me)(H)] can not be compared to published X-ray data of an analogous species, that is, a Zr–bis(indenyl)alkylhydride complex, since a Cambridge Structural Database (CSD)[30] search on such complexes yielded no results. However, the calculated structure is typical of a Zr$^{IV}$ complex of the type [Zr(Ind)$_2$X$_2$] and may be compared, for example, with the crystal structure of the dimethyl molecule (X = Me).[31] The optimised Zr–C distances are within 0.04 Å of the experimental values for the indenyl carbon atoms, and within 0.01 Å for the methyl ligand. For the pseudo-tetrahedral angles around the metal, X-Zr-X, the differences are 4° in the calculated and experimental structures.

The first mechanism investigated for the methane reductive elimination and the consequent formation of [Zr(Ind)$_2$] was one in which the structure of this complex was such that the two indenyl ligands have the relative conformation found in the THF adduct. This is a consecutive but distinct reaction known to occur after the alkane reductive elimination (see Scheme 1) and its product, [Zr($\eta^5$-Ind)($\eta^6$-Ind)-(thf)] was characterised by X-ray crystallography.[15] The relative orientation of the indenyl ligands in this complex corresponds to an *anti*-conformation of the two ligands ($\beta = 177°$) and, thus, the [Zr(Ind)$_2$] species with closest geometrical arrangement of the ligands is the *anti*-conformer of the $\eta^5/\eta^9$-complex, **A59**. The energy profile obtained for this mechanism is represented in Figure 6.

The mechanism in Figure 6 follows three steps. In the first step the relative conformation of the two Ind ligands goes from *gauche* in **A** to *anti* in **A′**, reaching the arrangement that exists in the product, **A59**. In the second step the Ind slips from a $\eta^5$ to a $\eta^6$, going through a transition state, **TS$_{A'B}$**, with the ligand coordinated in an intermediate geometry, and producing intermediate **B**, a species with one $\eta^5$-Ind and the other ligand coordinated by the benzene ring in a $\eta^6$-mode. The last step in Figure 6 mechanism corresponds to the methane reductive elimination from **B** and yields the final products, **A59** and methane. It is interesting to note that in the corresponding transition state, **TS$_{B-A59}$**, the slipping Ind is still rather planar and both the methyl carbon atom and the hydride are still coordinated to the metal. The system then evolves to the products by loosing methane and forming **A59**, with slippage of $\eta^6$-Ind to a $\eta^9$-mode, compensating the loss of the two ligands.

The overall activation energy for the mechanism represented in Figure 6 is rather high, 42.9 kcal mol$^{-1}$, and, therefore, an alternative process was investigated, in which the methane elimination occurs in the bis($\eta^5$-Ind) molecule, **A**. The corresponding energy profile is depicted in Figure 7.

The mechanism of Figure 7 includes two steps that concern the spin-singlet PES. In the first step there is elimination of methane producing a $\eta^2$-C–H adduct, **C**, which then

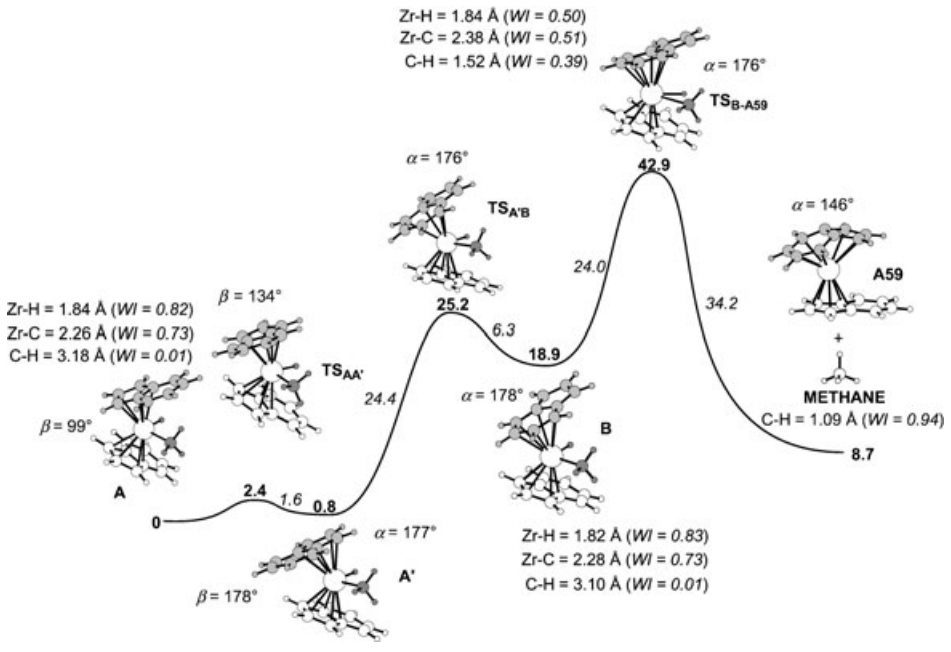


Figure 6. Energy profile for a mechanism of methane reductive elimination from [Zr($\eta^5$-Ind)$_2$(CH$_3$)(H)] (**A**) producing the *anti*-conformer of the [Zr($\eta^5$-Ind)($\eta^9$-Ind)] complex (**A56**). The minima and the transition states were optimised (B3LYP/VDZP) and the obtained structures are presented. The moving indenyl is shaded light grey and the hydride and the methyl groups, dark grey. The energies (kcal mol$^{-1}$) are referred to **A**, and the values in italics represent energy barriers. The more relevant geometrical parameters and Wiberg indices (italics) are presented.

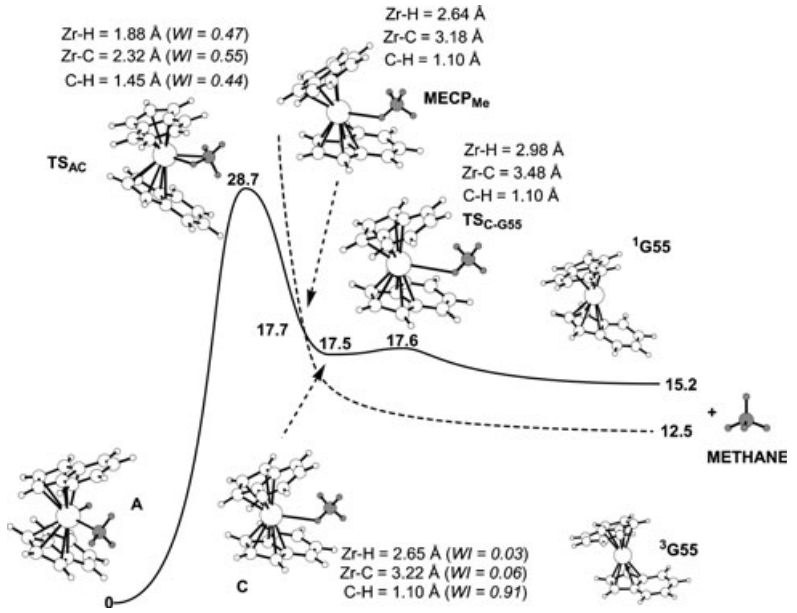


Figure 7. Energy profile for a mechanism of methane reductive elimination from $[Zr(\eta^5\text{-Ind})_2(CH_3)(H)]$ (**A**) producing the *gauche*-conformers of the $[Zr(\eta^5\text{-Ind})_2]$ intermediate (**G55**). The relevant points were optimised (B3LYP/VDZP) and the obtained structures are presented. The hydride and the methyl are shaded. The energies (kcal mol$^{-1}$) are referred to **A**, and the more relevant geometrical parameters and Wiberg indices (italics) are presented. The plain curve corresponds to the spin-singlet ($S=0$) PES and the dashed curve to the spin-triplet ($S=1$) PES.

dissociates to the products: methane and $[Zr(\eta^5\text{-Ind})_2]$, **$^1$G55**. However, given the existence of a more stable spin-triplet isomer of this species, **$^3$G55** (see above), the $S=1$ PES with the methane in the proximity of the Zr complex was searched, yielding the dashed curve in Figure 7, purely repulsive towards the formation of a triplet adduct. It should be noticed that the mechanism in Figure 7 is equivalent, in its general features, to the one previously obtained for the same reaction with $M(Cp)_2$ fragments, with M being a Group 6 metal.[32] An analysis of the spin-singlet surface (plain line in Figure 7) shows that the elimination step is closely related to the equivalent one in the previously discussed case (step 3 of the mechanism in Figure 6). The formation of the C–H bond occurs while both the hydride and the methyl are still coordinated to the metal (**TS$_{AC}$**) yielding a $\eta^2$-C–H adduct (**C**), with very loosely bound methane. In this species, the formation of the C–H bond is complete and the $CH_4$ moiety has practically the structure of free methane. In the last step, **C** dissociates into the products going through a very shallow transition state, **TS$_{C-G55}$** ($E_a=0.1$ kcal mol$^{-1}$), involving only minor structural changes. Since the spin-triplet species **$^3$G55** is more stable than its singlet analogue (see profile on the bottom of Figure 5) and the formation of a methane adduct with **$^3$G55** is unfavourable, with the corresponding PES being steadily repulsive as methane approaches the complex, then the two PESs have to cross. The MECP obtained (**MECP$_{Me}$**) presents a Zr–Me distance intermediate between **TS$_{AC}$** and **C**, but with a structure very similar to **C**. In fact, the three species corresponding to $\eta^2$-C–H adducts in Figure 7, **MECP$_{Me}$**, **C** and **TS$_{C-G55}$**, have very closely related geometries. The most important energy barrier and, thus, the rate-limiting step of the mechanism represented in Figure 7 is well determined (**TS$_{AC}$**), but one question is still open. What complex is formed, **$^3$G55** or **$^1$G55**? Or, in other words, how does the reaction occur, all the way through the singlet PES, or once the **MECP$_{Me}$** is reached does the system cross to the more stable triplet surface ending up in **$^3$G55**? It is not possible to have a final answer based solely on energy values, but some important considerations may arise from such analysis. On the one hand, the crossing point (**MECP$_{Me}$**) is easily attained from the $\eta^2$-C–H adduct, **C** (0.2 kcal mol$^{-1}$), but on the other hand **C** should have a very short lifetime, given the small energy barrier (0.1 kcal mol$^{-1}$) needed to overcome to yield the singlet products, **$^1$G55** and methane. Thus, although **MECP$_{Me}$** is easy to reach, the system should not be in its vicinity, from the geometrical point of view, for enough time to make this a viable path for a reaction and, therefore, it most probably follows the singlet PES all the way to the dissociation products. It is important to refer that whatever intermediate results from the methane elimination, **$^3$G55** or **$^1$G55**, the end dissociation product, as far as the metallic fragment is concerned, $[Zr(Ind)_2]$, will be the same. The profile in the bottom of Figure 5 will be followed yielding the most stable $[Zr(Ind)_2]$ isomer, that is, the $\eta^5/\eta^9$-complex in the *gauche*-conformation, **G59**. This is, in fact, the product of the reaction, experimentally identified[15] and fully characterised.[20] Besides, since the interconversion between the two $\eta^5/\eta^5$-species (**$^3$G55** and **$^1$G55**), going through **MECP$_{G55}$**, is easier than their isomerisation to **G59**, which has to go through **TS$_{G59-G55}$** (see the bottom profile of Figure 5 and its discussion above), both **$^3$G55** and **$^1$G55** will be intermediates in the methane reductive elimination, no matter which one will result directly from the Figure 7 profile.

The overall activation energy for the methane elimination following the mechanism represented in Figure 7 is 28.7 kcal mol$^{-1}$. To the best of our knowledge, there are no experimental values of activation parameters for this reaction with $[Zr(\eta^5\text{-Ind})_2(Me)(H)]$, but the ones measured for the corresponding reaction with related complexes, $[WCp_2(Me)(H)]$ ($\Delta H^{\neq}=25$ kcal mol$^{-1}$, $\Delta G^{\neq}_{298}=26$ kcal mol$^{-1}$)[33a] and $[ZrCp'_2(i\text{Bu})(H)]$ ($\Delta H^{\neq}=25$ kcal mol$^{-1}$, $\Delta G^{\neq}_{298}=24$ kcal mol$^{-1}$),[11,33b] compare remarkably well with the values calculated for the reaction represented in Figure 7: $\Delta H^{\neq}=\Delta G^{\neq}_{298}=28$ kcal mol$^{-1}$.

  

**Formation of the THF adduct [Zr(η⁵-Ind)(η⁶-Ind)(thf)]**: The THF adduct [Zr(η⁵-Ind′)(η⁶-Ind′)(thf)] was obtained by the reaction of the [Zr(Ind)$_2$] complex with THF ($C_4H_8O$), and was fully characterised by X-ray diffraction. This species includes indenyl ligands with $SiMe_3$ substituents at the $C_{b/b'}$ positions and played an important role for the understanding of the nature of the Zr sandwich complex.[15] The optimised geometry of the corresponding model, [Zr(η⁵-Ind)(η⁶-Ind)(thf)] (**D** in Figure 8), is in very good accordance with

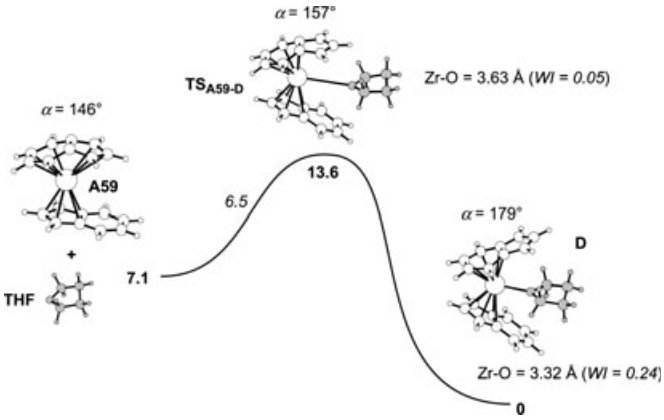


Figure 8. Energy profile for the mechanism of formation of the THF adduct, [Zr(η⁵-Ind)(η⁶-Ind)(thf)] (**D**), from **A59** and THF. The minima and the transition state were optimised (B3LYP/VDZP) and the obtained structures are presented. The energies (kcal mol$^{-1}$) are referred to **D**, and the value in italics represents the energy barrier. THF is shaded and the more relevant geometrical parameters and Wiberg indices (italics) are presented.

the experimental structure, given the differences between the two molecules, with mean and maximum absolute deviations of 0.04 and 0.10 Å for the bond lengths around the metal, and a 2° maximum difference for the relevant angles, L-Zr-L. One indenyl is coordinated in the common η⁵-mode, by means of the $C_5$ ring, while the other is bonded through the benzene ring in a η⁶-mode. The two ligands are aligned and have opposite benzene rings, in what may be called an *anti*-conformation, $\beta = 177°$(exptl) and 180°(calcd). The disposition of the indenyl ligands in the THF complex makes **A59**, the *anti*-conformer of the η⁵/η⁹-species, the most suitable [Zr(Ind)$_2$] complex to react with one molecule of THF and yield the final product. In fact, the two Ind ligands have exactly the same relative orientation in **A59** and in the product, [Zr(η⁵-Ind)(η⁶-Ind)(thf)]. Complex **A59** is readily accessible from the more stable conformer, **G59**, given the low activation energy involved in the rotation of the indenyl ligands of the bis(indenyl) species (see the energy profile in Figure 4).

The mechanism calculated for the formation of the THF adduct (Figure 8) is a very simple one, following just one step from the reactants, **A59** and THF, to the final product, [Zr(η⁵-Ind)(η⁶-Ind)(thf)] (**D**). The η⁹-Ind in **A59** dissociates the allylic part of the $C_5$ ring, opening a coordination position that will be occupied by the THF molecule. The transition state (**TS$_{A59-D}$**) is an early one, closest to the reactants than to the product, with a still significantly folded Ind ligand and a very incipient Zr–O bond, as shown by the corresponding geometrical parameters and Wiberg indices in Figure 8. The reaction is favourable, from a thermodynamic point of view ($\Delta E = -7.1$ kcal mol$^{-1}$), indicating that despite the saturated nature of the [Zr(Ind)$_2$] species **A59**, the steric constraints imposed by the η⁹-coordination geometry of one ligand produce a reactive species, and the system gains energy even by the formation of an adduct with a poor ligand such as THF. The activation energy calculated for the process ($E_a = 6.5$ kcal mol$^{-1}$) is easy to reach, in good accordance with a room-temperature reaction.[15]

The search for an analogue of **D** with the two indenyl ligands coordinated in a η⁵-mode yielded a spin-triplet species, [Zr(η⁵-Ind)$_2$(thf)] (**F**), 3.4 kcal mol$^{-1}$ more stable than its η⁵/η⁶-isomer **D**. The reasons for this stability difference are related to the Zr–Ind bond strength for the two indenyl coordination geometries, η⁵ and η⁶. As previously discussed for the [Zr(Ind)$_2$] species, a η⁶-Ind coordination mode normally results in a weaker Zr–Ind bond than a η⁵-Ind ligand and, consequently, in a less stable complex. The difference in the spin state of the two isomers is also easily explained (see Figure 9). A spin-triplet species is what would be expected for a d$^2$ bent metallocene with one donor ligand L. The frontier orbitals of such a molecule consist of two nearly degenerate nonbonding orbitals, $3a_1$ and $2b_1$, centred on the metal. The third frontier orbital for a bent metallocene, $4a_1$, will be involved in the bonding to the ligand L, THF in this case. The two metal electrons will be accommodated in two degenerate (or nearly so) orbitals and the result is a spin-triplet molecule. The nature of the orbital in-

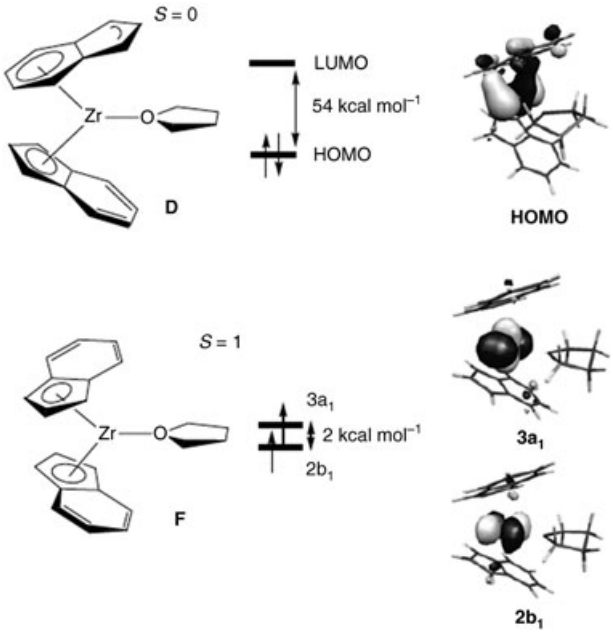


Figure 9. Frontier orbitals and energy splitting for [Zr(η⁵-Ind)(η⁶-Ind)(thf)] (**D**, top) and [Zr(η⁵-Ind)$_2$(thf)] (**F**, bottom).

teractions between the metal and the benzene ring of a $\eta^6$-Ind justifies the spin-singlet state of **D**. The establishment of a $\delta$ interaction between $3a_1$ and the coordinated benzene ring breaks the degeneracy of the frontier orbitals and yields a spin-singlet molecule. The resulting molecular orbital (HOMO) is similar to what is found for the [Zr($\eta^5$-Ind)-($\eta^9$-Ind)] species (see Figure 2).

Since the bis($\eta^5$-Ind) isomer **F** is more stable than the $\eta^5$/$\eta^6$-complex **D**, a final question remains to be answered: why is **D** the experimentally obtained product? The answer is provided by the energy profile of Figure 10.

There are two limiting paths for the conversion of [Zr($\eta^5$-Ind)($\eta^6$-Ind)(thf)] (**D**) into is $\eta^5$/$\eta^5$-triplet isomer, **F**. One is to cross from the singlet PES to the triplet surface directly from **D**. This is represented in the right side of Figure 10 and in the first step **D** has to reach the $\mathbf{MECP_{DE}}$ overcoming a 20.6 kcal mol$^{-1}$ barrier and yielding the triplet complex **E**. In this step the $\eta^6$-Ind slips to a $\eta^5$-coordination, maintaining the relative orientation of the two Ind ligands as the system moves from the singlet to the triplet surfaces. At the crossing point, $\mathbf{MECP_{DE}}$, the slipping ligand is slightly folded and its coordination is practically $\eta^5$; the Zr–$C_a$ bond is almost formed (2.81 Å), while the Zr–$C_{d/d'}$ and the Zr–$C_{e/e'}$ bonds are already broken (2.90 and 3.41 Å, respectively). Once the triplet intermediate **E** is reached the rotation of the indenyl occurs smoothly, through a transition state $\mathbf{TS_{EF}}$, which is practically isostructural with **E** and without significant activation energy, resulting in the product **F**. In the second path, represented on the left side of Figure 10, the Ind slippage and rotation occurs in the singlet surface, yielding a singlet species **H**, with a geometry analogous to that in product **F**. Then the system crosses to the triplet surface, producing **F** in a final step. The Ind slippage from $\eta^6$ to $\eta^5$ has a 20.6 kcal mol$^{-1}$ barrier, corresponding to $\mathbf{TS_{DG}}$. This transition state has a geometry very similar to $\mathbf{MECP_{DE}}$, discussed above, with a slightly folded ligand and the $\eta^5$-coordination mode of the slipping ligand almost reached (Zr–$C_a$ = 2.81 Å, Zr–$C_{d/d'}$ = 2.94 Å and Zr–$C_{e/e'}$ = 3.44 Å). The complex formed (**G**), a spin-singlet bis($\eta^5$-Ind) species, is only 0.9 kcal mol$^{-1}$ less stable than **D**. The Ind ligand in **G** rotates in order to attain the conformation present in the final product. This rotation step occurs smoothly ($E_a$ = 0.7 kcal mol$^{-1}$) and the corresponding transition state, $\mathbf{TS_{GH}}$, presents a geometry intermediate between **G** and the resulting complex, **H**, a $\eta^5$/$\eta^5$-singlet molecule with a geometry very similar to the one existing in **F**. Interestingly, **H** is 0.6 kcal mol$^{-1}$ more stable than the original isomer, [Zr($\eta^5$-Ind)($\eta^6$-Ind)(thf)] (**D**), both being singlet molecules. The final product, **F**, is obtained by a hopping of the system from the singlet PES to the triplet surface, via $\mathbf{MECP_{FH}}$, a crossing point with a geometry in between **H** and **F**. The small energy barrier involved (0.4 kcal mol$^{-1}$) reflects the negligible structural arrangements needed to obtain $\mathbf{MECP_{FH}}$ from **H**.

The energy profile in Figure 10 indicates that **D** is enclosed in a potential well, and the activation energy (20.6 kcal mol$^{-1}$) needed to yield the more stable isomer **F** is apparently out of reach under the experimental conditions. The more stable spin-triplet species, [Zr($\eta^5$-Ind)$_2$(thf)] (**F**), could, in principle, be obtained warming the reaction mixture, through the mechanisms represented in Figure 10. However, decomposition takes place upon heating the THF adduct, and C–O bond cleavage is observed.[34]

It is important to recall here that, experimentally, the methane elimination and the formation of the THF adduct correspond to two separate reactions, and the [Zr($\eta^5$-Ind)-($\eta^9$-Ind)] complex, equivalent to **G59**, was actually isolated[15] and fully characterised.[20] Once **G59** is formed, the most favourable path to the formation of a THF adduct leads to the singlet complex, **D** (right side of Figure 11).

Another possibility of obtaining **F**, at least from the theoretical point of view, would be to carry the alkane elimination in the presence of THF. Should that be the case and the

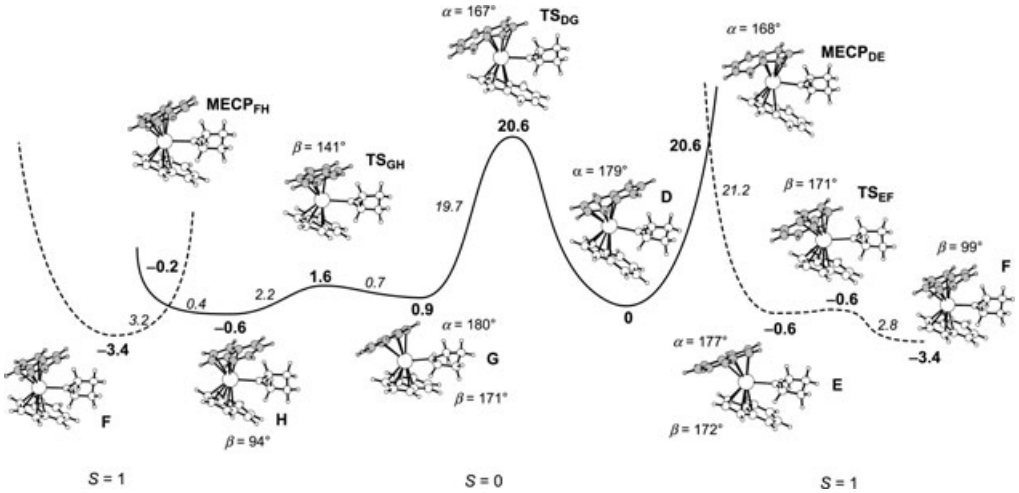


Figure 10. Energy profile for the conversion of [Zr($\eta^5$-Ind)($\eta^6$-Ind)(thf)] (**D**) into [Zr($\eta^5$-Ind)$_2$(thf)] (**F**). The relevant points were optimised (B3LYP/VDZP) and the obtained structures are presented. The energies (kcal mol$^{-1}$) are referred to **D**, and the values in italics represent energy barriers. The moving indenyl is shaded and the relevant angles ($\alpha$ and $\beta$) are indicated. The plain curves correspond to the spin-singlet ($S$ = 0) PES and the dashed curves to the spin-triplet ($S$ = 1) PES.

  

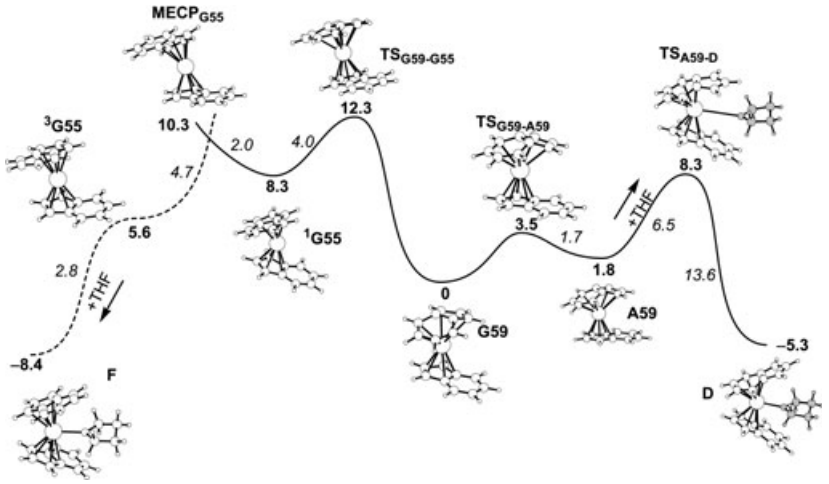


Figure 11. Energy profile for the formation of the two THF adducts (**D** and **F**) from the [Zr(Ind)$_2$] complexes. The minima and the transition states were optimised (B3LYP/VDZP) and the obtained structures are presented. The energies (kcal mol$^{-1}$) are referred to **G59**, and the values in italics represent energy barriers. The plain curve corresponds to the spin-singlet ($S=0$) PES and the dashed curve to the spin-triplet ($S=1$) PES.

$\eta^5/\eta^5$-intermediate resulting from the elimination, **$^1$G55** or **$^3$G55** (see Figure 7), may be trapped forming the more stable triplet adduct **F** (left side of Figure 11). In fact, **$^1$G55** converts more easily to its triplet analogue **$^3$G55** ($E_a=$ 2.0 kcal mol$^{-1}$) than to **G59** ($E_a=4.0$ kcal mol$^{-1}$). In addition, a thorough search of the PES for the reaction of **$^3$G55** with THF yielded a completely attractive curve towards the formation of **F**, and no transition state could be located. Nevertheless, the small activation energy needed to reach the more stable isomer **G59** from **$^1$G55** can make the trapping of **$^3$G55** by THF a difficult task, from the experimental point of view. On the other hand, the discussion above and the corresponding conclusions should be taken with some caution given the small energy differences involved. The validity of the theoretical model used may be crucial, since the electronic and steric influence of the substituents on the $C_{b/b'}$ atoms of indenyl, present in the experimental study, may change considerably the relative energies of the relevant species, such as different isomers, transition states or MECP. For example, in a recent work, Hanusa et al.[35] found that $SiMe_3$ or *t*Bu on those same positions of Ind change the preferred conformation of [Cr(Ind)$_2$], favouring a low spin state.

## Conclusion

The zirconium sandwich species [Zr($\eta^5$-Ind)($\eta^9$-Ind)] are saturated 18-electron Zr$^{II}$ complexes with one indenyl ligand in a $\eta^9$-coordination mode, with participation of its entire $\pi$ system in the bonding to the metal and becoming a 10-electron donor. The indenyl rotation in these molecules is easy, but the interchange process of the two ligands requires higher activation energies, following a path involving $\eta^5/\eta^5$-intermediates with two symmetrically coordinated $\eta^5$-Ind.

The methane reductive elimination in the alkylhydride complexes occurs directly in the bis($\eta^5$-Ind) species, [Zr($\eta^5$-Ind)$_2$(CH$_3$)(H)], producing a [Zr($\eta^5$-Ind)$_2$] complex that then evolves the more stable $\eta^5/\eta^9$-isomer, following a mechanism in which the rate-limiting step is the first one.

The formation of the THF adduct, [Zr($\eta^5$-Ind)($\eta^6$-Ind)-(thf)] occurs in a one step mechanism, from [Zr($\eta^5$-Ind)-($\eta^9$-Ind)] with the two indenyl ligands in the right conformation. The complex experimentally obtained, [Zr($\eta^5$-Ind)($\eta^6$-Ind)(thf)], has a more stable isomer, the bis($\eta^5$-Ind) complex with spin-triplet state. The high activation energies involved on the isomerisation prevents this process from occurring under experimental conditions.

It is important to note that the participation of the benzo portion of the indenyl ligand in bonding to a metal, producing a geometrical distortion similar to the $\eta^9$-coordination found in the bis(indenyl) complex, may be responsible for the stabilisation of electron-deficient intermediates, explaining the long known increased reactivity of indenyl complexes, with respect to their cyclopentadienyl analogues, even for reactions that follow dissociative pathways.[36]

## Computational Methods

All calculations were performed by using the Gaussian 98 software package,[37] and the B3LYP hybrid functional, without symmetry constraints. That functional includes a mixture of Hartree–Fock[38] exchange with DFT[16] exchange correlation, given by Becke's three-parameter functional[17] with the Lee, Yang and Parr correlation functional, which includes both local and non-local terms.[18,19] The LanL2DZ basis set[39,40] augmented with an f-polarisation function[41] was used for Zr, and a standard 6–31G(d,p)[42] for the remaining elements. This basis set is denoted VDZP. Transition-state optimisations were performed with the synchronous transit-guided quasi-Newton method (STQN) developed by Schlegel et al.[43] Frequency calculations were performed to confirm the nature of the stationary points, yielding one imaginary frequency for the transition states and none for the minima. Each transition state was further confirmed by following its vibrational mode downhill on both sides, and obtaining the minima presented on the energy profiles. The energy values presented on the reaction profiles were not zero-point corrected, since, on the one hand the maximum deviation between the zero-point corrected and the uncorrected energies was 1 kcal mol$^{-1}$ for all the stationary points, and, on the other the MECP are not stationary points and a standard frequency analysis is not applicable.[44] However, the enthalpies and free energies discussed along the text only involve stationary points and were obtained, at 298.15 K and 1 atm, by conversion of the zero-point-corrected electronic energies with the thermal energy corrections based on the calculated structural and vibrational frequency data. A natural population analysis (NPA)[28] and the resulting Wiberg indi-

ces[21] were used for a detailed study of the electronic structure and bonding of the optimised species. Spin contamination was carefully monitored for all the unrestricted calculations performed for the triplet species and the open shell singlets, that is, all the $\eta^5/\eta^5$-species with $S=0$, but a more stable triplet state. The values of $\langle S^2\rangle$ indicate minor spin contamination and are presented in the Supporting Information. The minimum energy crossing points (MECP) between the spin-singlet ($S=0$) and the spin-triplet ($S=1$) potential energy surfaces (PES) were determined by using a code developed by Harvey et al.[44] This code consists of a set of shell scripts and Fortran programs that uses the Gaussian results of energies and gradients of both spin states to produce an effective gradient pointing towards the MECP. The orbital drawings were obtained using the program MOLEKEL 4.0.[45]

The basis set convergence, in size, was tested through the optimisation of selected examples of the studied species with a valence triple-zeta basis set with added polarisation functions (VTZP), consisting of the Stuttgart/Dresden ECP (SDD)[46] basis set with an extra f-polarisation function[41] for Zr, and a standard 6–311G(d,p)[47] for the remaining elements. The geometries obtained at this level are identical to the ones obtained with the smaller basis set (B3LYP/VDZP), and the differences in the relative energies calculated with the two theoretical models are accordingly small, even when different spin states are compared. For example, the energy difference between the spin-triplet $\eta^5/\eta^5$-[Zr(Ind)$_2$] intermediate ($^3$**G55**) and its $\eta^6/\eta^9$-spin-singlet isomer (**G69**), both in the *gauche*-conformation, is 7.8 kcal mol$^{-1}$ with the B3LYP/VDZP model and drops to 7.3 kcal mol$^{-1}$ for the molecules optimised with the VTZP basis set. This difference of 0.5 kcal mol$^{-1}$ is perfectly suitable for the discussion here intended.

The most accurate functional to describe energy differences between states of different spin in organo-transition-metal complexes is still a matter of discussion. Although the hybrid functionals, such as B3LYP, can be a good choice in many cases, their 20% admixture of exact exchange has been shown to overestimate the stability of higher spin states in some systems. Modified hybrid functionals with 15% exact exchange have been proposed, yielding better results in what concerns the energy splitting between different spin states, especially for first-row transition-metal complexes.[48,49] To test the dependence of the system here studied on the amount of exact exchange used in the functional, some chosen examples of the complexes described were recalculated by using a modified B3LYP functional with 15% admixture of exact exchange (B3LYP*). The geometries optimised with the modified B3LYP* functional were identical to those obtained with the "normal" B3LYP. The same happened with the energy splitting between species with the same spin state. For example, the difference in the relative energies for [Zr($\eta^5$-Ind)($\eta^9$-Ind)] (**G59**) and [Zr($\eta^6$-Ind)($\eta^9$-Ind)] (**G69**), optimised with the two functionals was only 0.1 kcal mol$^{-1}$. However, slightly larger differences were found in the relative stability of molecules with different spin states. As expected,[48] B3LYP tends to favour spin triplets with respect to singlets, when compared to B3LYP*. For example, the energy difference between the *gauche*-conformers of [Zr($\eta^5$-Ind)$_2$] ($^3$**G55**) and [Zr($\eta^5$-Ind)($\eta^9$-Ind)] (**G59**) increased from 5.6 kcal mol$^{-1}$, for the B3LYP optimised complexes, to 7.5 kcal mol$^{-1}$ when B3LYP* was used. This represents a difference of 1.9 kcal mol$^{-1}$ for the energy splitting between the two isomers, depending on the amount of exact exchange included in the functional. Similar values were obtained for the THF adduct. In this case, B3LYP* single-point calculations were carried on B3LYP optimised geometries. The stability differences between singlet [Zr($\eta^5$-Ind)($\eta^6$-Ind)(thf)] (**D**) and triplet [Zr($\eta^5$-Ind)$_2$(thf)] (**F**) were 3.4 (B3LYP) and 1.8 kcal mol$^{-1}$ (B3LYP*). Here, the triplet was the most stable species and, again, the tendency of B3LYP to favour the triplet state was noted with a difference of 1.6 kcal mol$^{-1}$ on the relative stability of the two complexes, depending on the functional. Although the system studied reveals some dependence on the amount of exact exchange included in the functional, the difference on the energy splitting is not too significant ($<2$ kcal mol$^{-1}$), and the use of B3LYP/VDZP geometries and energies along the text seems adequate for the semi-quantitative discussion presented. This conclusion is reinforced by two reasons. The first is that even with the noted tendency of B3LYP to favour the spin-triplet species, in the end these were not found to play an active part on the more favourable reaction mechanisms proposed. The second, and perhaps more strong argument, is the excellent agreement between the calculated activation parameters and the experimental data available for the alkane reductive elimination and for the interconversion process between the two indenyl ligands in the [Zr(Ind)$_2$] complex.

## Acknowledgements

The author is thankful to Dr. Paul J. Chirik, for calling his attention to this problem and for sharing data prior to publication, and also to Dr. Jeremy N. Harvey for the granting of the code for MECP determination, as well as by many explanations crucial to overcome the difficulties and pitfalls of DFT calculations involving molecules with different spin states, and the optimisation of MECP. The referees are acknowledged for pertinent and most helpful comments.

[1] R. H. Crabtree, *The Organometallic Chemistry of the Transition Metals*, 3rd ed., Wiley, New York, **2001**, p. 129.
[2] E.-I. Negishi, T. Takahashi, *Acc. Chem. Res.* **1994**, *27*, 124.
[3] a) M. D. Fryzuk, *Chem. Rec.* **2003**, *3*, 2; b) M. D. Fryzuk, S. A. Johnson, *Coord. Chem. Rev.* **2000**, *200*, 379.
[4] U. Rosenthal, P.-M. Pellny, F. G. Kirchbauer, V. V. Burkalov, *Acc. Chem. Res.* **2000**, *33*, 119.
[5] H. H. Brintzinger, J. E. Bercaw, *J. Am. Chem. Soc.* **1970**, *92*, 6182.
[6] a) D. H. Berry, L. J. Procopio, P. J. Carroll, *Organometallics* **1988**, *7*, 570; b) T. E. Hanna, E. Lobkovsky, P. J. Chirik, *J. Am. Chem. Soc.* **2004**, *126*, 14688.
[7] P. B. Hitchcock, F. Kerton, G. A. Lawless, *J. Am. Chem. Soc.* **1998**, *120*, 10264.
[8] L. Lukesová, M. Horácek, P. Stepnicka, K. Fejfarová, R. Gyepes, I. Cisorová, J. Kubista, K. Mach, *J. Organomet. Chem.* **2002**, *663*, 134.
[9] M. Horácek, V. Kupfer, U. Thewalt, P. Stepnicka, M. Polásek, K. Mach, *Organometallics* **1999**, *18*, 3572.
[10] M. Horácek, P. Stepnicka, J. Kubista, K. Fejfarová, R. Gyepes, K. Mach, *Organometallics* **2003**, *22*, 861.
[11] J. A. Pool, E. Lobkovsky, P. J. Chirik, *J. Am. Chem. Soc.* **2003**, *125*, 2241.
[12] K. I. Gell, J. Schwartz, *J. Am. Chem. Soc.* **1981**, *103*, 2687.
[13] J. M. O'Connor, C. P. Casey, *Chem. Rev.* **1987**, *87*, 307.
[14] For a recent reinterpretation of the indenyl effect and a comprehensive reference list on the subject, see: M. J. Calhorda, C. C. Romão, L. F. Veiros, *Chem. Eur. J.* **2002**, *8*, 868.
[15] C. A. Bradley, E. Lobkovsky, P. J. Chirik, *J. Am. Chem. Soc.* **2003**, *125*, 8110.
[16] R. G. Parr, W. Yang, *Density Functional Theory of Atoms and Molecules*, Oxford University Press, New York, **1989**.
[17] A. D. Becke, *J. Chem. Phys.* **1993**, *98*, 5648.
[18] B. Miehlich, A. Savin, H. Stoll, H. Preuss, *Chem. Phys. Lett.* **1989**, *157*, 200.
[19] C. Lee, W. Yang, G. Parr, *Phys. Rev. B* **1988**, *37*, 785.
[20] C. A. Bradley, I. Keresztes, E. Lobkovsky, V. G. Young, P. J. Chirik, *J. Am. Chem. Soc.* **2004**, *126*, 16937.
[21] a) K. B. Wiberg, *Tetrahedron* **1968**, *24*, 1083; b) Wiberg indices are electronic parameters related with the electron density in between two atoms. They can be obtained from a natural population analysis and provide an indication on the bond strength.
[22] K. Jonas, P. Korb, G. Kollbach, B. Gabor, R. Mynott, K. Angermund, O. Heineman, C. Krüger, *Angew. Chem.* **1997**, *109*, 1793; *Angew. Chem. Int. Ed. Engl.* **1997**, *36*, 1714.
[23] T. A. Albright, P. Hofmann, R. Hoffmann, C. P. Lillya, P. A. Dobosh, *J. Am. Chem. Soc.* **1983**, *105*, 3396.
[24] K. Costuas, J.-Y. Saillard, *Chem. Commun.* **1998**, 2047.
[25] G. Erker, K. Engel, C. Krueger, A.-P. Chiang, *Chem. Ber.* **1982**, *115*, 3311.

  

[26] J. C. Green, M. L. H. Green, G. C. Taylor, J. Saunders, *J. Chem. Soc. Dalton Trans.* **2000**, 317.
[27] J. C. Green, *Chem. Soc. Rev.* **1998**, *27*, 263.
[28] a) J. E. Carpenter, F. Weinhold, *J. Mol. Struct. THEOCHEM* **1988**, *169*, 41; b) J. E. Carpenter, Ph.D. thesis, University of Wisconsin (Madison WI), **1987**; c) J. P. Foster, F. Weinhold, *J. Am. Chem. Soc.* **1980**, *102*, 7211; d) A. E. Reed, F. Weinhold, *J. Chem. Phys.* **1983**, *78*, 4066; e) A. E. Reed, F. Weinhold, *J. Chem. Phys.* **1983**, *78*, 1736; f) A. E. Reed, R. B. Weinstock, F. Weinhold, *J. Chem. Phys.* **1985**, *83*, 735; g) A. E. Reed, L. A. Curtiss, F. Weinhold, *Chem. Rev.* **1988**, *88*, 899; h) F. Weinhold, J. E. Carpenter, *The Structure of Small Molecules and Ions*, Plenum, **1988**, 227.
[29] For excellent reviews on MECP and their location for transition-metal complexes, see: a) J. N. Harvey, R. Poli, K. M. Smith, *Coord. Chem. Rev.* **2003**, *238/239*, 347; b) R. Poli, J. N. Harvey, *Chem. Soc. rev.* **2003**, *32*, 1.
[30] F. H. Allen, *Acta Crystallogr. Sect. B* **2002**, *58*, 380.
[31] a) J. L. Atwood, W. E. Hunter, D. C. Hrncir, E. Samuel, H. Alt, M. D. Rausch, *Inorg. Chem.* **1975**, *14*, 1757; b) The structure optimised for $[Zr(\eta^5\text{-Ind})_2(Me)(H)]$ compares also very well with the X-ray structure of $[Zr(\eta^5\text{-Ind}')(\eta^5\text{-Ind}'')(i\text{Pr})(H)]$ with substituted indenyls, $Ind' = C_9H_6t\text{Bu}$, $Ind'' = C_9H_5(SiMe_3)_2$ (P. J. Chirik, unpublished results). The experimental distances for the Zr–C(indenyl) bonds are within 0.07 Å of the calculated values, the corresponding differences being 0.02 Å for the ancillary ligands, Zr–C(*i*Pr) and Zr–H. The calculated L-Zr-L angles are within 2° of the experimental ones.
[32] J. C. Green, J. N. Harvey, R. Poli, *J. Chem. Soc. Dalton Trans.* **2002**, 1861.
[33] a) R. M. Bullock, C. E. L. Headford, K. M. Hennessy, S. E. Kegley, J. R. Norton, *J. Am. Chem. Soc.* **1989**, *111*, 3897; b) In the case of the Zr complex, the reductive elimination of alkane is followed by oxidative addition of a C–H bond of one of the Cp′ substituents, yielding a cyclometalated product (see ref. [11]). The agreement between calculated and experimental activation parameters suggests that alkane elimination is the rate-determining step.
[34] P. J. Chirik, personal communication.
[35] E. D. Brady, J. S. Overby, M. B. Meredith, A. B. Mussman, M. A. Cohn, T. P. Hanusa, G. T. Yee, M. Pink, *J. Am. Chem. Soc.* **2002**, *124*, 9556.
[36] a) A. J. Hart-Davis, R. J. Mawby, *J. Chem. Soc. A* **1969**, 2403; b) C. White, R. J. Mawby, *Inorg. Chim. Acta* **1970**, *4*, 261; c) C. White, R. J. Mawby, A. J. Hart-Davis, *Inorg. Chim. Acta*, **1970**, *4*, 441; d) D. J. Jones, R. J. Mawby, *Inorg. Chim. Acta* **1972**, *6*, 157; e) L.-N. Ji, M. E. Rerek, F. Basolo, *Organometallics* **1984**, *3*, 740; f) R. M. Kowalesky, D. O. Kipp, K. J. Stauffer, P. N. Swepston, F. Basolo, *Inorg. Chem.* **1985**, *24*, 3750; g) N. N. Turaki, J. M. Huggins, L. Lebioda, *Inorg. Chem.* **1988**, *27*, 424.
[37] Gaussian 98, Revision A.7, M. J. Frisch, G. W. Trucks, H. B. Schlegel, G. E. Scuseria, M. A. Rob, J. R. Cheeseman, V. G. Zakrzewski, J. A. Montgomery, Jr., R. E. Stratmann, J. C. Burant, S. Dapprich, J. M. Millam, A. D. Daniels, K. N. Kudin, M. C. Strain, O. Farkas, J. Tomasi, V. Barone, M. Cossi, R. Cammi, B. Mennucci, C. Pomelli, C. Adamo, S. Clifford, J. Ochterski, G. A. Petersson, P. Y. Ayala, Q. Cui, K. Morokuma, D. K. Malick, A. D. Rabuck, K. Raghavachari, J. B. Foresman, J. Cioslowski, J. V. Ortiz, A. G. Baboul, B. B. Stefanov, G. Liu, A. Liashenko, P. Piskorz, I. Komaromi, R. Gomperts, R. L. Martin, D. J. Fox, T. Keith, M. A. Al-Laham, C. Y. Peng, A. Nanayakkara, C. Gonzalez, M. Challacombe, P. M. W. Gill, B. Johnson, W. Chen, M. W. Wong, J. L. Andres, C. Gonzalez, M. Head-Gordon, E. S. Replogle, and J. A. Pople, Gaussian, Pittsburgh PA, **1998**.
[38] W. J. Hehre, L. Radom, P. v. R. Schleyer, J. A. Pople, *Ab Initio Molecular Orbital Theory*, Wiley, NY, **1986**.
[39] T. H. Dunning, Jr., P. J. Hay, *Modern Theoretical Chemistry*, *Vol. 3* (Ed.: H. F. Schaefer III), Plenum, New York, **1976**, p. 1.
[40] a) P. J. Hay, W. R. Wadt, *J. Chem. Phys.* **1985**, *82*, 270; b) W. R. Wadt, P. J. Hay, *J. Chem. Phys.* **1985**, *82*, 284; c) P. J. Hay, W. R. Wadt, *J. Chem. Phys.* **1985**, *82*, 2299.
[41] A. W. Ehlers, M. Böhme, S. Dapprich, A. Gobbi, A. Höllwarth, V. Jonas, K. F. Köhler, R. Stegmann, A. Veldkamp G. Frenking, *Chem. Phys. Lett.* **1993**, *208*, 111.
[42] a) R. Ditchfield, W. J. Hehre, J. A. Pople, *J. Chem. Phys.* **1971**, *54*, 724; b) W. J. Hehre, R. Ditchfield, J. A. Pople, *J. Chem. Phys.* **1972**, *56*, 2257; c) P. C. Hariharan, J. A. Pople, *Mol. Phys.* **1974**, *27*, 209; d) M. S. Gordon, *Chem. Phys. Lett.* **1980**, *76*, 163; e) P. C. Hariharan, J. A. Pople, *Theor. Chim. Acta* **1973**, *28*, 213.
[43] a) C. Peng, P. Y. Ayala, H. B. Schlegel, M. J. Frisch, *J. Comput. Chem.* **1996**, *17*, 49; b) C. Peng, H. B. Schlegel, *Isr. J. Chem.* **1993**, *33*, 449.
[44] J. N. Harvey, M. Aschi, H. Schwarz, W. Koch, *Theor. Chem. Acc.* **1998**, *99*, 95.
[45] P. Flükiger, H. P. Lüthi, S. Portmann, J. Weber, Swiss Center for Scientific Computing, Manno (Switzerland), **2000**.
[46] a) U. Haeusermann, M. Dolg, H. Stoll, H. Preuss, *Mol. Phys.* **1993**, *78*, 1211; b) W. Kuechle, M. Dolg, H. Stoll, H. Preuss, *J. Chem. Phys.* **1994**, *100*, 7535; c) T. Leininger, A. Nicklass, H. Stoll, M. Dolg, P. Schwerdtfeger, *J. Chem. Phys.* **1996**, *105*, 1052.
[47] a) A. D. McClean, G. S. Chandler, *J. Chem. Phys.* **1980**, *72*, 5639; b) R. Krishnan, J. S. Binkley, R. Seeger, J. A. Pople, *J. Chem. Phys.* **1980**, *72*, 650; c) A. J. H. Wachters, *J. Chem. Phys.* **1970**, *52*, 1033; d) P. J. Hay, *J. Chem. Phys.* **1977**, *66*, 4377; e) K. Raghavachari, G. W. Trucks, *J. Chem. Phys.* **1989**, *91*, 1062; f) R. C. Binning, L. A. Curtiss, *J. Comput. Chem.* **1995**, *103*, 6104; g) M. P. McGrath, L. Radom, *J. Chem. Phys.* **1991**, *94*, 511.
[48] J. N. Harvey, *Struct. Bonding* **2004**, *112*, 1.
[49] J. N. Harvey, M. Aschi, *Faraday Discuss.* **2003**, *124*, 129.

Received: December 2, 2004
Published online: February 24, 2005